ACS APPLIED NANO MATERIALS
Cite This: ACS Appl. Nano Mater. XXXX, XXX, XXX−XXX
Article
www.acsanm.org

Silver-Nanoparticle-Embedded Porous Silicon Disks Enabled SERS Signal Amplification for Selective Glutathione Detection

Yang Bu,[†,‡,⊥] Guixian Zhu,[‡,§,⊥] Shengliang Li,[‡] Ruogu Qi,[‡] Gauri Bhave,[‡] Dechen Zhang,[‡,∥] Ruixuan Han,[‡] Dali Sun,[‡] Xiangfeng Liu,[†] Zhongbo Hu,[†] and Xuewu Liu*[,‡]

[†]College of Materials Sciences and Optoelectronics, University of Chinese Academy of Sciences, Beijing 100049, China
[‡]Department of Nanomedicine, Houston Methodist Research Institute, Houston, Texas 77030, United States
[§]School of Instrument Science and Optoelectronics Engineering, Beijing Information Science and Technology University, Beijing 100192, China
[∥]Key Laboratory for Molecular Enzymology & Engineering, The Ministry of Education, College of Life Science, Jilin University, Jilin 130012, China

Supporting Information

ABSTRACT: As the major redox couple and nonprotein thiol source in human tissues, the level of glutathione (GSH) has been a concern for its relation with many diseases. However, the similar physical and chemical properties of interference molecules such as cysteine (Cys) and homocysteine (Hcy) make discriminative detection of GSH in complex biological fluids challenging. Here we report a novel surface-enhanced Raman scattering (SERS) platform, based on silver-nanoparticle-embedded porous silicon disks (PSDs/Ag) substrates for highly sensitive and selective detection of GSH in biofluids. Silver nanoparticles (AgNPs) were reductively synthesized and aggregated directly into pores of PSDs, achieving a SERS enhancement factor (EF) up to 2.59×10^7. Ellman's reagent 5,5′-ditho-bis (2-nitrobenzoic acid) (DTNB) was selected as the Raman reactive reporting agent, and the GSH quantification was determined using enzymatic recycling method, and allowed the detection limit of GSH to be down to 74.9 nM using a portable Raman spectrometer. Moreover, the significantly overwhelmed enhancement ratio of GSH over other substances enables the discrimination of GSH detection in complex biofluids.

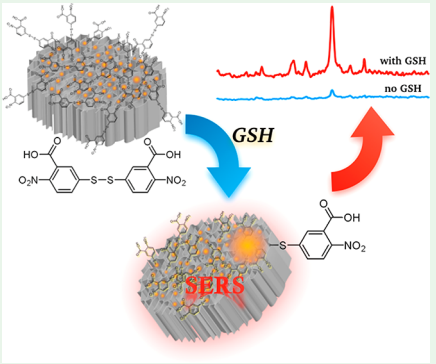

KEYWORDS: *biosensor, porous silicon, silver nanoparticles, SERS, glutathione, signal amplification*

INTRODUCTION

As the main nonprotein cellular thiol, glutathione (GSH) exists in most mammalian tissues with an approximate concentration of 0.5−10 mM in cells and biological tissues.[1] The tripeptide, in the form of reduced GSH and oxidized GSH, maintains intracellular thiol−disulfide balance to adjust various biological processes.[2] Also, as an essential antioxidant, the thiol functional group in GSH captures toxic metal ions and harmful free radicals.[3] Therefore, a variety of diseases are closely associated with GSH deficiency such as cancers, HIV progressions, and Parkinson's diseases.[4−6] Consequently, its significant biological role drives the need of the GSH level's assessment in biological systems.[7−10] However, other biothiols such as cysteine (Cys) and homocysteine (Hcy) hold similar physical and chemical properties as compared to GSH, which makes their selective detection challenging. The conventional methods generally use techniques such as high-performance liquid chromatography (HPLC), electrochemistry, and colorimetry.[11−13] HPLC requires sophisticated time-consuming manipulations; electrochemical probes with complex electrode modifications lack stability, and colorimetry methods suffer from relatively low sensitivity (∼1 μM). Recently, fluorescence spectroscopy and electrochemiluminescence methods have been developed rapidly and achieve higher sensitivity and selectivity in biosensing.[14−19] For example, the 4,4-difluoro-4-bora-3a,4a-diaza-s-indacene-based (BODIPY-based) fluorescent probes emit fluorescence signals upon encountering GSH, which enables the differentiation of GSH from Cys and Hcy.[20] However, the molecular fluorescent probes require a tedious synthesis procedure, and the fluorescent bioimaging in real samples suffers from background interference. Semiconductor quantum-dot-based fluorescent probes are concerning because of their potential toxicity; electrochemiluminescence-based methods require a complicated procedure of luminophore preparation, which limits its application in clinical use.[21,22] Thus, there still exists an urgent need for the development of novel and simple methods for GSH detection.

Since the first observation of pyridine on the electrochemically roughened Ag electrode, surface-enhanced Raman scattering (SERS) has been continuously developed and

Received: December 3, 2017
Accepted: December 18, 2017
Published: December 18, 2017

DOI: 10.1021/acsanm.7b00290
ACS Appl. Nano Mater. XXXX, XXX, XXX−XXX

dramatically explored in molecular detection.[23−27] Even though enhanced SERS detection sensitivity of biomolecules benefits from aggregated noble metal (gold, silver, and copper) nanoparticles, the insufficient enhancement factor (EF) and poor stability caused by not well-defined structures limit the SERS applications. Therefore, the fabrication of an arrayed structure for the controllable nanostructure's gap distance has been widely investigated.[28−30] Xu et al. have shown that nanoparticles with sub-10 nm space distance have almost 10^{10} SERS enhancement on molecules.[31] However, the development of uniformed metal nanoclusters with a proper gap distance between the neighboring nanostructure remains challenging. Another possible method to produce abundant hot spots and enhance the SERS signal is by adopting a nanosurface with roughness, and the correlation between surface roughness and plasmon intensity has been proven and studied.[32,33] However, the complicated fabrication process for demanding nanostructured SERS substrates results in higher cost and lower reproducibility. Porous silicon (pSi) materials hold a great potential in biosensing and drug delivery, for their larger surface-to-volume ratio, easier chemical modification, and biodegradable features.[34,35] The pSi's reducibility also enables the metal deposition with the oxidation of silicon to SiO_2 and provides a promising matrix for structural support to control the spacing between metal nanoparticles formed and aggregated in the porous structure.[36−38] Such hybrid particles also produce a rough surface, which exhibits intense hot spots for SERS detection. To overcome the self-fluorescence disturbance which limits SERS application in direct detections of biomolecules, various reporting-agent-based indirect methods have been developed by researchers, using Raman active molecules such as rhodamine 6G (R6G), 4-mercaptobenzoic acid (MBA), Prussian blue (PB), and crystal violet (CV).[39−42] 5,5′-Dithio-bis(2-nitrobenzoic acid) (DTNB), being not just an Ellman's reagent to detect thiols in solutions, also plays the role as a Raman reporter.[43−45] A typical colorimetric method first explored by Frank Tietze utilized the thiol−disulfide exchange reaction between GSH and the sulfhydryl reagent DTNB, and the enzymic method for determining GSH concentration was based on catalytic action of reduced GSH in reducing DTNB with TPNH and yeast glutathione reductase.[46] The produced Raman active 2-nitro-5-thiobenzoate (TNB^{2-}) has absorption at 412 nm, which was monitored by a plate reader, and also leaves the possibility to monitor the GSH level by SERS detections.

Here in this study, a novel SERS platform was developed, based on silver-nanoparticle-embedded porous silicon disks (PSDs/Ag) substrates for highly sensitive and selective detection of GSH. Aggregated silver nanoparticles (AgNPs) were synthesized directly into pores by the PSDs' reducibility; (3-aminopropyl) triethoxysilane (APTES) was applied as the capping agent for controlling the morphology of silver nanoparticles as well as surface functional ligands. Subsequently, various surface modifications, reagent concentrations, and volumes were adjusted to optimize the conditions for the SERS detection. DTNB was used as the Raman reporter, and shows activity toward thiols by producing Raman active TNB^{2-} with a SERS signal enhancement ratio, which can be used for quantitative study. For realization of the sensitive and discriminative detection of GSH in complex biological fluids, the enzymatic recycling method using glutathione reductase (GR) and dihydronicotinamide-adenine dinucleotide phosphate (NADPH) was adopted, to validate the analysis of GSH in PBS and human serum.

EXPERIMENTAL SECTION

Materials and Reagents. Silver nitrate, APTES, poly(sodium 4-styrenesulfonate) solution (average $M_w \sim 70\,000$, 30 wt % in H_2O), poly(allylamine hydrochloride) (average M_w 50 000), 5,5′-ditho-bis (2-nitrobenzoic acid), β-nicotinamide adenine dinucleotide phosphate reduced, yeast glutathione reductase, L-glutathione reduced, L-cysteine, L-homocysteine, L-arginine, L-histidine, L-isoleucine, L-leucine, L-lysine, L-methionine, L-phenylalanine, L-threonine, L-tyrosine, and L-valine were purchased from Sigma-Aldrich. P-type wafer was purchased from Silicon Quest (Santa Clara, CA). Isopropyl alcohol (IPA) and phosphate buffered saline were purchased from Fisher Scientific. All chemicals are reagent grade, and deionized water was obtained from a Milli-Q ultrapure (18.2 MΩ cm) system.

Fabrication of Mesoporous Silicon Microparticles. PSDs (porous silicon disks, 1000 (diameter) × 400 (thickness) nm, pore size ranges from 20 to 60 nm) were produced by the combination of photolithography and electrochemical etching according to our group's previously reported protocol.[47] Briefly, starting with a p-type wafer with resistivity of 0.005 Ω cm as the substrate, the wafer was exposed to 1:3 HF (49%)/ethanol solution, and electrochemically etched with a dc current density of 16 mA/cm^2 for 45 s to form a 400 nm thick porous silicon layer. The current density was then jumped to 76 mA/cm^2, and kept for 6 s to form a second porous layer, the high-porosity release layer. After deposition of 80 nm thick low-temperature oxide (LTO) on the porous film, photolithography process was carried out using an i-line contact aligner (KARL SUSS MA6) and NR9-500P photoresist (Futurrex, Franklin, NJ). The patterns were transferred into the double-layer porous films by a Reactive Ion Etch instrument in CF4 plasma (Plasmatherm BatchTop). After stripping the LTO in dilute HF, the monodisperse PSDs were released by ultrasound in isopropyl alcohol (IPA).

Synthesis, Modification, and Characterization of PSDs/Ag Composites. A simple synthesis of PSDs/Ag composites was realized by applying the reducibility of porous silicon disks (PSDs). Briefly, 20 μL of 40 mM silver nitrate ($AgNO_3$) aqueous solution was added in 1 mL of PSD (particle number = 1.5×10^8) suspension containing 20 μL of APTES in IPA. After 30 min of reaction under ultrasonication, the formed composites were centrifuged at 13 000g and washed thoroughly by IPA three times. Finally, the composites were stored in 1 mL of IPA. PSDs were quantified by using a Coulter counter (Beckman Mutisizer 4). For evaluation of the influence of surface charges on the SERS effect of PSDs/Ag composites, poly(sodium 4-styrenesulfonate) (PSS) and poly(allylamine hydrochloride) (PAH) were applied to modify PSDs/Ag composites. Briefly, after centrifugation, PSDs/Ag composites were vacuum pumped to remove excess IPA; then 0.5% (w/v) PSS and PAH aqueous solutions were added separately and stirred for 90 min. The modified PSDs/Ag composites were washed by deionized (Milli-Q) water three times and finally restored in IPA before SERS measurement.

The morphology of PSDs/Ag composites was characterized by a Nova Nano scanning electron microscopy 230 instrument (SEM, high vacuum, HV = 8 kV, spot size 3.5) and a JEM-2100 field emission gun transmission electron microscope (TEM). A UV−vis spectrometer (DU730, Beckman Coulter) was applied to measure the absorption spectra. The surface ζ potential of PSDs/Ag composites was determined by a Zetasizer Nano (Malvern) instrument.

Surface-Enhanced Raman Spectroscopy Measurement. GSH, Cys, and Hcy standard solutions with various concentrations diluted by Milli-Q water/PBS/human serum were prepared. In this work, DTNB was used as Raman reporter for SERS detections; DTNB was dissolved in deionized water at a variety of concentrations (ranging from 10^{-3} to 10^{-9} M) and stored in the dark before use. For the determination of the analyte's concentration, 10 μL of 100 μM DTNB was mixed with 10 μL of analyte, and then, 4 μL of GR/NADPH (1:1) was added to this mixture; after 30 min of incubation at 37 °C, this was mixed with 10 μL of PSDs/Ag composites (particle

DOI: 10.1021/acsanm.7b00290
ACS Appl. Nano Mater. XXXX, XXX, XXX−XXX

Scheme 1. Schematic Illustrations of PSDs/Ag Composites as the Substrates in SERS Measurements: (a) In-Pore Synthesis of Silver Nanoparticles, and (b) SERS Signal Amplification for GSH Detection

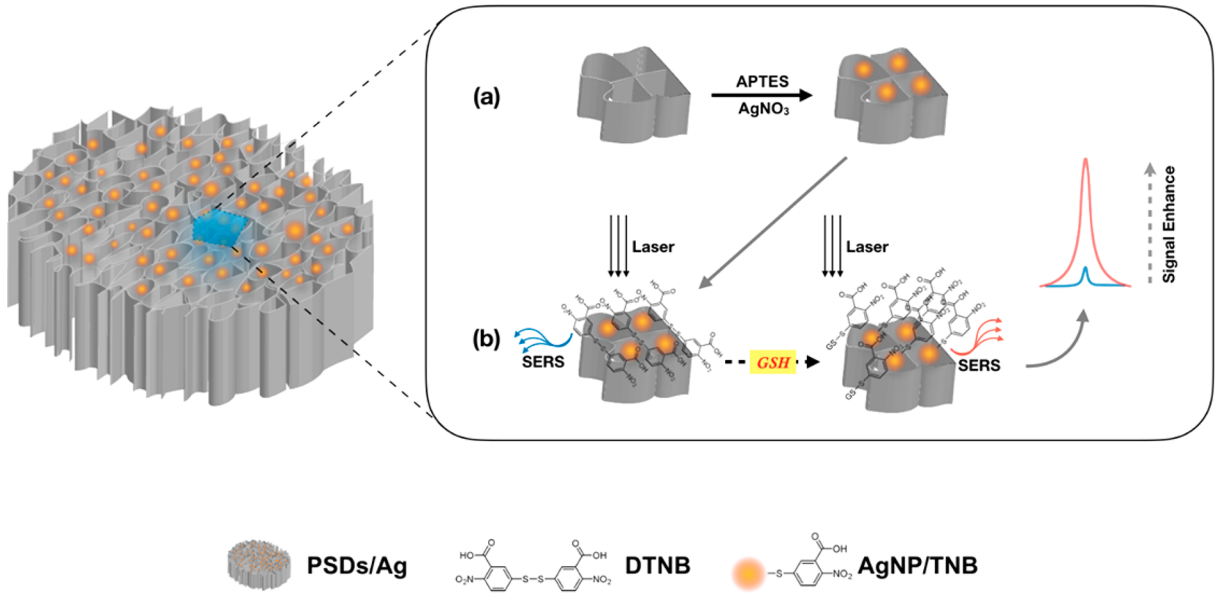

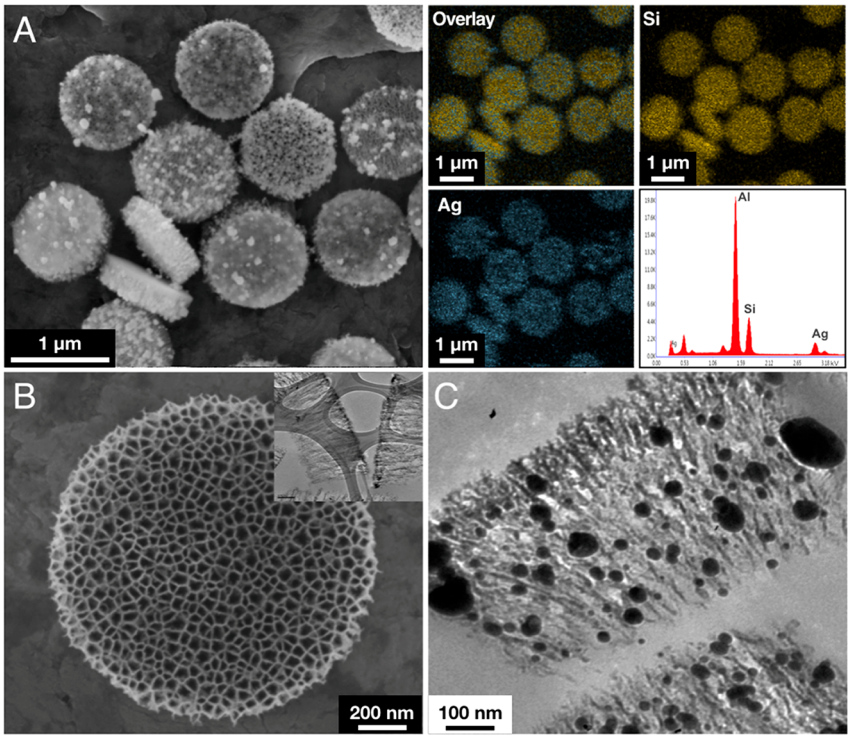

Figure 1. (A) SEM and EDS element mapping images of PSDs/Ag composites. (B) SEM/TEM images of PSDs and (C) TEM image of PSDs/Ag composite 70 nm slices (porous silicon filled with Ag nanoparticles).

number = 3.75 × 10^5) thoroughly before taken to SERS measurements.

Biologically relevant amino acids including L-arginine, L-histidine, L-isoleucine, L-leucine, L-lysine, L-methionine, L-phenylalanine, L-threonine, L-tyrosine, and L-valine were selected as the interference molecules. Typically, each of these amino acids including GSH, Cys, and Hcy was mixed with 10 μL of 10^{-4} M DTNB and 4 μL of GR/NADPH (1:1), and incubated for 30 min at 37 °C. Next, the SERS measurement was performed as described above. All Raman spectra were obtained using a portable Raman spectrometer (StellarNet, Inc.) with a 785 nm laser system operating at a power of 350 mW. The exposure time for each sample was set to a fixed 5 s accumulation. Triplicate measurement was conducted for each sample.

RESULTS AND DISCUSSION

Sensing Strategy and Optimization of the PSDs/Ag SERS Platform. The sensing strategy toward GSH is depicted in Scheme 1. The PSDs/Ag SERS substrates were fabricated by using a simple one-step deposition process. Silver ions were reduced directly into pores by taking advantage of pSi's reducibility, forming aggregated silver-nanoparticle-embedded

DOI: 10.1021/acsanm.7b00290
ACS Appl. Nano Mater. XXXX, XXX, XXX−XXX

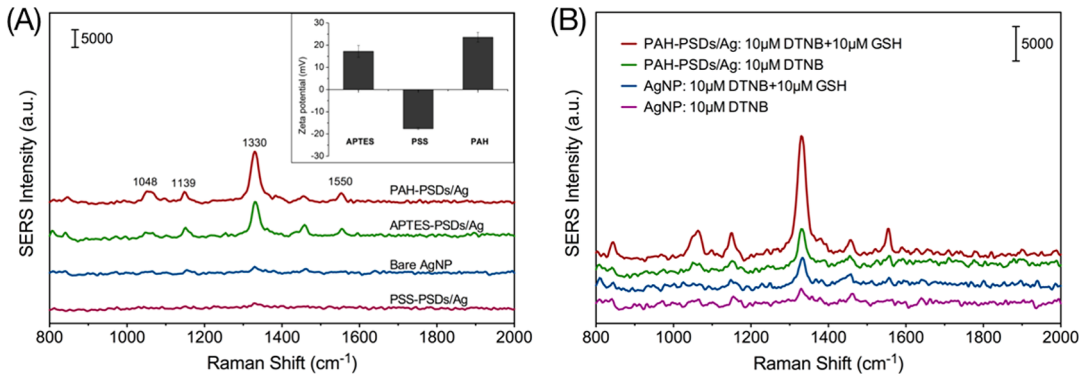

Figure 2. (A) Influence of different surface charges on SERS spectra of 100 μM DTNB solution with PSDs/Ag mixture. Inset figure: the ζ potential of PSDs/Ag composites with different surface modifications. (B) SERS spectra of 10 μM DTNB solution with PAH−PSDs/Ag mixture before and after adding standard 10 μM GSH. Radiation of a 785 nm laser was applied for excitation, and exposure time was set to a single 5 s accumulation.

porous silicon disks (PSDs/Ag). The silver deposition process can be explained by the following equations:[38]

$$Si + 2H_2O \rightarrow SiO_2 + 4H^+ + 4e^- \quad \text{(oxidation)} \quad (1)$$

$$Ag^+ + e^- \rightarrow Ag \quad \text{(reduction)} \quad (2)$$

The pSi performed as not only a reducing agent but also a vector that guaranteed the aggregated state of silver nanoparticles because the porous structure bordered the reaction sites. As previously reported, the morphology and size distribution of metal nanoparticles have an impact on the SERS effect of substrates.[48] Here, the uniformed hierarchical nanoporous structure of our well-defined PSDs forms a controlled nanoscale roughness and restricts the distribution (size and spacing) of aggregated silver nanoparticles. Applied as the capping agent, the APTES controls the morphology of silver nanoparticles as well as surface functional ligands, affecting SERS performance. Here, the optimized APTES concentration (20 μL in 1 mL of IPA) was adopted through an optimization process to maximize the Raman signal of 100 μM DTNB. As shown in the Supporting Information (Figure S1), the amount of APTES is critical for forming suitable particle size and aggregation degree of the silver nanoparticles by providing numerous nucleation sites for the silver growth; excessive volume of APTES results in the blockage of pore structure, thereby preventing the in-pore formation of silver nanoparticles. The concentration of $AgNO_3$ precursor solution was further optimized (Figure S2); the size of in-pore-synthesized silver nanoparticles increases with higher $AgNO_3$ concentration, and the corresponding SERS signal of 100 μM DTNB achieved the maximum when 40 mM $AgNO_3$ was added to the deposition process. Redundant $AgNO_3$ fails to grow silver nanoparticles inside the pore structure, as shown in Figure S2. Under the optimized condition, the SEM and EDS images shown in Figure 1A indicate that the silver nanoparticles (diameter, 20−60 nm) were well-distributed in the porous silicon matrix in the form of an aggregated status. The large surface area of PSDs improves the capability of absorbing silver ions into the pores, thereby forming abundant silver nanoparticle aggregates for SERS detection. Meanwhile, the penetration depth at a Raman excitation wavelength of 785 nm can reach at least several hundred nanometers into silicon, which makes the laser penetrable through the silicon porous disks, enabling the silver nanoparticles inside the pores to serve the SERS function.[49] In addition, the ∼10 nm wall thickness of silicon nanopores implements the stationary distance between the neighboring silver nanoparticles (Figure 1B,C). The property of mesoporous silicon, which enables the reduction of various noble metal ions from solutions, simplified the synthesis procedure, as the silver ions were reduced directly in the PSD matrix by reducibility of porous silicon. On the basis of the enzymatic recycling method raised by Frank Tietze, the thiol−disulfide exchange reaction between GSH and DTNB forms TNB and GS-TNB, and then, GS-TNB is reduced by GR and NADPH with the generation of GSH and TNB, which specifically recycles the GSH to generate more TNB for the signal amplification and enables selective GSH detection over other biothiols.[46] In neutral or alkaline water solution, TNB can be ionized to Raman reactive TNB^{2-} dianions. Therefore, the PSDs/Ag substrates were modified to alter its surface ζ potential easily to adsorb analyte with various charges. Here, for the selective GSH detection, positively charged PSDs/Ag substrates were specially designed for adsorbing TNB^{2-} dianions to the surface through their electrostatic interaction, leading to an intensity increase of the SERS signal. The intensity differences (enhancement ratios) were then used for quantification of GSH concentration.

For further optimization toward SERS detection, the as-prepared PSDs/Ag composites were modified with PSS or PAH to test the influence of surface charges on SERS spectra of DTNB. Figure 2A shows the ζ potential of PSDs/Ag composites in PBS solution (pH = 7.4) under different surface modifications; the results indicate that the surface charge of PSDs/Ag composites exhibited an impact on SERS spectra of DTNB molecules. After addition of DTNB (pI = 3.5) to PSDs/Ag composite solution, the SERS signal was dominated because the negatively charged DTNB in PBS (pH = 7.4) could easily bind to the substrate's surface. The influence of pH value was further investigated in the Supporting Information (Figure S3); results show that the neutral or weak alkaline environment serves as the ideal condition for DTNB detection. Compared with negatively charged PSS-modified PSDs/Ag (denoted as PSS−PSDs/Ag) composites, the PAH-modified PSDs/Ag (denoted as PAH−PSDs/Ag) composites with positive surface charge exhibited a much stronger SERS effect; the optimization of PAH concentration used for surface modification was achieved, as shown in the Supporting Information (Figure S4). Moreover, the PAH−PSDs/Ag composites showed higher SERS signal intensities than APTES-modified ones. Meanwhile, free silver nanoparticles showed the weakest signals among the composite substrates. The peaks of DTNB molecules at 1330 and 1550

DOI: 10.1021/acsanm.7b00290
ACS Appl. Nano Mater. XXXX, XXX, XXX−XXX

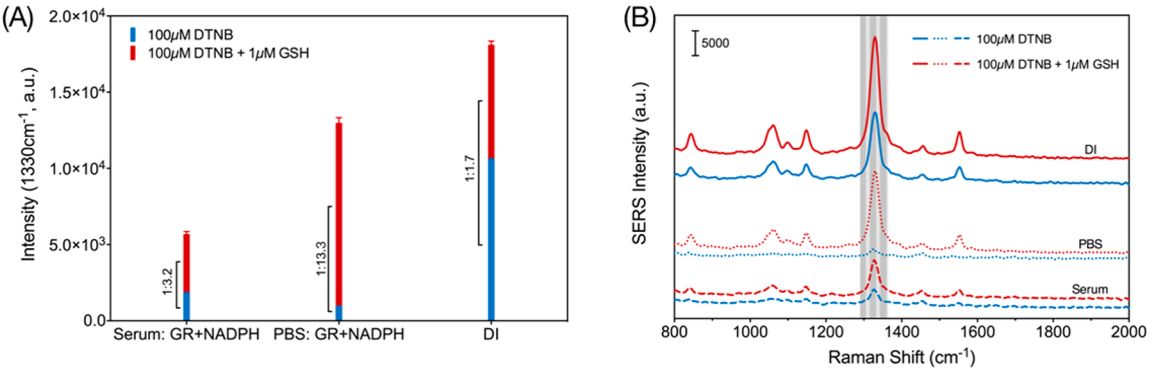

Figure 3. (A) Validation of PSDs/Ag substrates in detecting GSH in human serum, PBS, and DI. The blue bars designate the SERS intensities of 100 μL DTNB, and the red bars designate the SERS intensities after DTNB-GSH reaction. SERS signal enhancement ratios were calculated from the mean values. (B) Corresponding Raman spectra for GSH detection in DI, PBS, and human serum; characteristic 1330 cm^{-1} peaks are indicated by the shaded box. All measurements were conducted in triplicate.

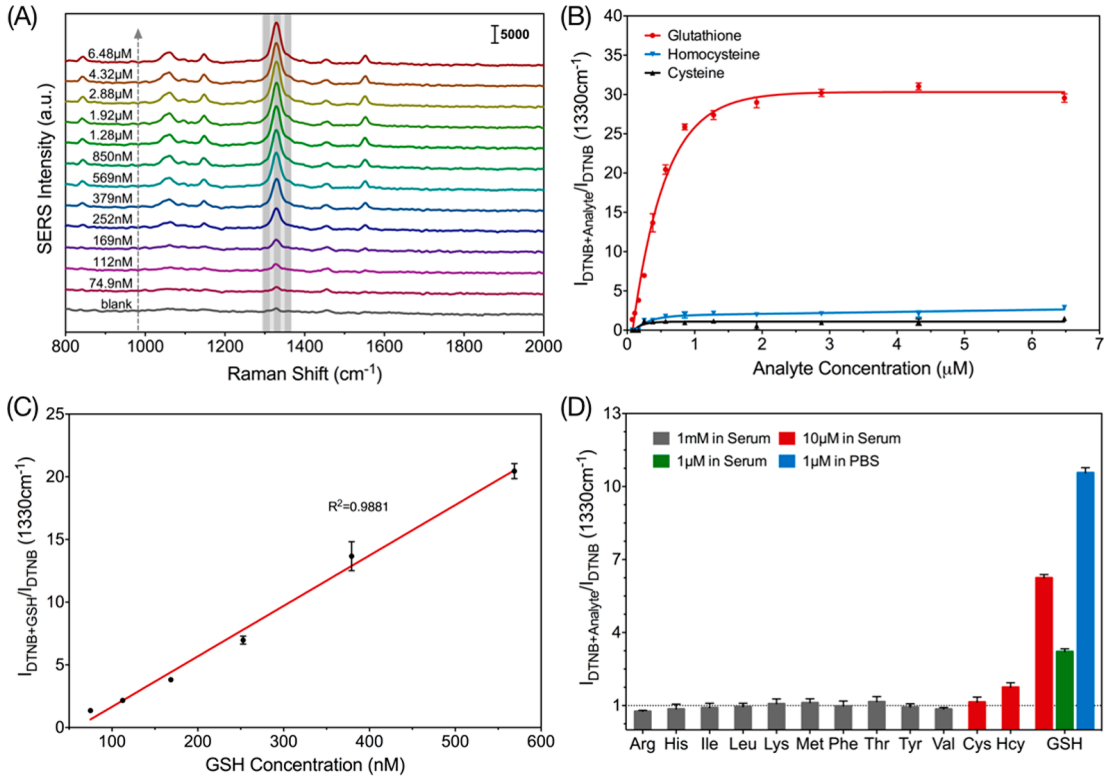

Figure 4. (A) Raman signal intensities increase along with the increase in GSH concentrations. (B) SERS signal enhancement ratio against concentration profile of GSH/Cys/Hcy detected using PSDs/Ag as the substrates. (C) Variation of SERS signal enhancement ratio at 1330 cm^{-1} with the GSH concentration in the low-concentration region. (D) SERS signal enhancement ratios of 10 μM GSH, Cys, and Hcy, and 1 mM arginine, histidine, isoleucine, leucine, lysine, methionine, phenylalanine, threonine, tyrosine, and valine were calculated from Raman spectra obtained from the enzymatic recycling method with PSDs/Ag as the SERS substrates. Blue bar: 1 mM GSH-spiked serum diluted 1000 times by 1× PBS. All measurements were conducted in triplicate.

cm^{-1} represent symmetric nitro stretch vs NO_2 and an aromatic ring stretching mode, separately. CH_3 rocking and C−N stretching and bending were reflected at 1139 and 1048 cm^{-1} on the Raman spectrum. Notably, the Raman signal at 1330 cm^{-1} was extremely enhanced after GSH addition (Figure 2B). The Raman signal's enhancement occurs with the cleavage of equimolar DTNB into two TNB^{2-} molecules by the thiol band in GSH in the alkaline environment. The generation of cleaved TNB^{2-} after the addition of GSH provides the Raman reporting signal source; the TNB^{2-} can be adsorbed to aggregated silver nanoparticles and the PAH-modified positively charged surface along with the enormous surface area enlarge the adsorption capacity, thus enhancing the Raman signal, while no significant changes in active peak positions were found. Therefore, it is beneficial to apply PAH−PSDs/Ag as the SERS substrates in the measurement of bioactive molecules, and the signal differences of DTNB before and after reaction with thiol groups can be adopted for quantification of thiol-containing molecules. For investigation of the influence of PAH−PSDs/Ag's concentration on the SERS signal of DTNB, Raman spectra were collected, and the highest peaks at 1330 cm^{-1} were used for presenting SERS

DOI: 10.1021/acsanm.7b00290
ACS Appl. Nano Mater. XXXX, XXX, XXX−XXX

intensities (height value = $I_{1330} - I_{1304}$; Figure S5A). There was an optimal ratio between amounts of PSDs/Ag composites and DTNB molecules where the identical peak reached the highest value when there was 20 μL of PAH−PSDs/Ag composites in the mixture (Figure S5B). The PSDs/Ag SERS platform showed a limit of detection (LOD) of 10 nM toward DTNB molecules (Figure S6); the SERS signal variation was also observed from the SERS signal distribution of 15 repeated experiments as shown in Figure S7, demonstrating that the PAH surface modification improves reproducibility as well as signal intensities. A time-dependence test of signal stability ranging from 0 to 72 h in Figure S7C proves a higher stability than conventional AgNPs. The magnitude of EF in the detection of DTNB was calculated according to the equation EF = $(I_{SERS}N_{Raman})/(N_{SERS}I_{Raman})$, in which I_{SERS} and I_{Raman} are intensities for SERS and normal Raman signals at 1330 cm^{-1}, respectively; N_{Raman} and N_{SERS} are the number of DTNB molecules contributing to normal Raman and SERS signals. The calculated value of EF is 2.59×10^7 for the SERS detection of DTNB under the optimized condition.

SERS Signal Enhancement Effect. For determination of the GSH's concentration under the enzymatic recycling method using GR and NADPH, the observed SERS intensities were recorded against incubation time from 0 to 90 min as shown in Figure S8. The figure shows that the SERS intensities of the GSH group ascend gradually and reach the plateau after 30 min of incubation at 37 °C, while the Cys group remains at a lower level throughout until 90 min. The signal difference proves the formation of TNB^{2-} under the existence of GR and NADPH, which indicates the distinct specificity toward GSH detection of this method. As previously discussed, the signal enhancement caused by the enzymatic recycling-reaction-generated TNB^{2-} can be used for quantitative determination of GSH's concentration. For validation of the signal enhancement effect, measurements under different solution environments were carried out, as shown in Figure 3. In deionized water, 100 μM pure DTNB exhibits a higher SERS signal than in serum or PBS, which is ascribed to the more efficient adsorption of DTNB to the PSDs/Ag substrates in the simpler solution system. After incubation for 30 min with GR and NADPH, the signal enhancement ratios (calculated as $I_{DTNB+GSH}/I_{DTNB}$ at 1330 cm^{-1}) achieve 13.3 in PBS, and 3.2 in human serum, respectively. A ratio of only 1.7 was achieved by direct reaction of DTNB and GSH in deionized water. In complex solution systems (PBS/serum), the DTNB molecules are less prone to bind to the PAH−PSDs/Ag substrates. The TNB^{2-} dianions generated from DTNB during the thiol−disulfide exchange reaction then bound to surface positively charged PAH−PSDs/Ag substrates via the strong electrostatic interaction, leading to a significant SERS signal enhancement, which enables quantitative measurements of analytes with higher sensitivity in complex biofluids.

Sensitivity and Selectivity of the PSDs/Ag SERS Platform. For an investigation of the sensitivity of the PSDs/Ag SERS platform in detection of GSH in PBS using the enzymatic recycling method, a GSH standard solution of certain concentration was spiked and diluted with PBS to gradient concentrations. For demonstration of the selectivity of this method toward GSH over other interference molecules, Cys and Hcy samples are included as well. For quantitative measurements, SERS spectra were collected after 30 min of incubation at 37 °C for each sample. Particularly, the signal intensities as a function of the GSH concentrations are demonstrated in Figure 4A, which increase along with the increase in GSH concentrations. The SERS signal enhancement ratios were calculated as $I_{DTNB+GSH}/I_{DTNB}$ at 1130 cm^{-1}, and the relationship between concentrations of analyte (GSH, Cys, or Hcy) and SERS enhancement ratios was plotted, as shown in Figure 4B. The plot shows a rapid increase of signal enhancement ratio, which approaches a saturated plateau at an analyte concentration higher than 3 μM. This trend presents similarly for GSH, Cys, and Hcy, while GSH exhibits a much higher signal enhancement ratio than the other two, which indicates the specific detection toward GSH using this method. Figure 4C shows a linear response to GSH concentrations in PBS against SERS signal enhancement. GSH concentrations lower than 568.9 nM produce a good linear relation, with a regression coefficient $R^2 = 0.9881$, and the estimated detection limit for GSH in PBS with the PSDs/Ag SERS platform is 74.9 nM, which is lower than that for the conventional colorimetric method (~1 μM). The specific enzymatic recycle method generates more TNB for the signal amplification and enables selective GSH detection over other biothiols. The positively charged surface in our proposed method is specially designed for adsorbing negatively charged substances including the TNB^{2-}. As shown in Figure 4D, for the diminishment of interference of other substances in complex biofluids, the blue bar indicates the process of treating serum samples by diluting with PBS, acquiring better sensing sensitivity with a higher signal enhancement ratio. The dilution process can also be adopted for real samples with high GSH concentrations. For further investigation on the selectivity for the detection of GSH in human serum, several biologically relevant amino acids including L-arginine, L-histidine, L-isoleucine, L-leucine, L-lysine, L-methionine, L-phenylalanine, L-threonine, L-tyrosine, and L-valine were chosen as the interference molecules, and were spiked in human serum to achieve 1 mM solutions, then examined using the proposed method. Their SERS signal enhancement ratios were calculated along with Cys, Hcy, and GSH spiked human serum samples, as shown in Figure 4D. The result reveals that the PSDs/Ag SERS-based platform displays unique selectivity toward GSH over Cys/Hcy and other amino acids in human serum, which holds great potential for GSH detection in complex biological samples.

CONCLUSION

We have developed a novel SERS platform for the highly sensitive and selective detection of GSH, based on PSDs/Ag as the SERS substrates fabricated with a simple synthesis process. The well-defined porous silicon disks with uniformed hierarchical porous structure form a controlled nanoscale roughness of aggregated silver nanoparticles, which provides a high SERS enhancement factor. The large surface area of PSDs improves the capability of adsorbing silver ions into the pores, thereby forming abundant silver nanoparticles aggregated for SERS detection and providing more reaction sites for analyte molecules. We demonstrated that the thiol group's specific interaction with DTNB that produces Raman active TNB^{2-} exhibits the SERS signal enhancement effect, and the signal enhancement ratios were calculated for the quantitative determination of the analytes. By adoption of the enzymatic recycling method using GR and NADPH, higher SERS enhancement ratios for GSH were achieved over Cys/Hcy, allowing a detection limit of 74.9 nM in PBS. This platform was further applied toward the validation of selectivity for the

DOI: 10.1021/acsanm.7b00290
ACS Appl. Nano Mater. XXXX, XXX, XXX−XXX

detection of GSH over other substances in human serum, showing its potential for GSH detection in vivo.

■ ASSOCIATED CONTENT

Supporting Information

The Supporting Information is available free of charge on the ACS Publications website at DOI: 10.1021/acsanm.7b00290.

Characterization, optimization and stability details, SEM images, UV−vis spectra, ζ potential, and Raman spectra (PDF)

■ AUTHOR INFORMATION

Corresponding Author

*E-mail: xliu@houstonmethodist.org.

ORCID

Yang Bu: 0000-0003-2448-4743
Shengliang Li: 0000-0002-3890-8482
Ruogu Qi: 0000-0001-9222-9272
Dechen Zhang: 0000-0003-3984-7674
Xiangfeng Liu: 0000-0001-9633-7721
Xuewu Liu: 0000-0002-8702-0295

Author Contributions

⊥Y.B. and G.Z. contributed equally to this work. The manuscript was written through contribution of all authors. All authors have given approval to the final version of the manuscript.

Notes

The authors declare no competing financial interest.

■ ACKNOWLEDGMENTS

The authors thank Dr. Jianhua Gu for his help in SEM imaging. Microfabrication of PSD was performed at the Microelectronics Research Center at the University of Texas at Austin. The authors acknowledge financial support from the following sources: Grants NIH 1R21CA190024-01, DOD W81XWH-12-1-0414, National Natural Science Foundation of China Grant 81571791, and the Houston Methodist Research Institute.

■ REFERENCES

(1) Maher, P. The Effects of Stress and Aging on Glutathione Metabolism. *Ageing Res. Rev.* **2005**, *4*, 288−314.

(2) Townsend, D. M.; Tew, K. D.; Tapiero, H. The Importance of Glutathione in Human Disease. *Biomed. Pharmacother.* **2003**, *57*, 145−155.

(3) Ceballos-Picot, I.; Witko-Sarsat, V.; Merad-Boudia, M.; Nguyen, A. T.; Thévenin, M.; Jaudon, M. C.; Zingraff, J.; Verger, C.; Jungers, P.; Descamps-Latscha, B. Glutathione Antioxidant System as a Marker of Oxidative Stress in Chronic Renal Failure. *Free Radical Biol. Med.* **1996**, *21*, 845−853.

(4) Balendiran, G. K.; Dabur, R.; Fraser, D. The Role of Glutathione in Cancer. *Cell Biochem. Funct.* **2004**, *22*, 343−352.

(5) Herzenberg, L. A.; De Rosa, S. C.; Dubs, J. G.; Roederer, M.; Anderson, M. T.; Ela, S. W.; Deresinski, S. C.; Herzenberg, L. A. Glutathione Deficiency Is Associated with Impaired Survival in HIV Disease. *Proc. Natl. Acad. Sci. U. S. A.* **1997**, *94*, 1967−1972.

(6) Spina, M. B.; Cohen, G. Dopamine Turnover and Glutathione Oxidation: Implications for Parkinson Disease. *Proc. Natl. Acad. Sci. U. S. A.* **1989**, *86*, 1398−1400.

(7) Dieckhaus, C. M.; Fernandez-Metzler, C. L.; King, R.; Krolikowski, P. H.; Baillie, T. A. Negative Ion Tandem Mass Spectrometry for the Detection of Glutathione Conjugates. *Chem. Res. Toxicol.* **2005**, *18*, 630−638.

(8) Lakritz, J.; Plopper, C. G.; Buckpitt, A. R. Validated High-Performance Liquid Chromatography-Electrochemical Method for Determination of Glutathione and Glutathione Disulfide in Small Tissue Samples. *Anal. Biochem.* **1997**, *247*, 63−68.

(9) Tian, D.; Qian, Z.; Xia, Y.; Zhu, C. Gold Nanocluster-Based Fluorescent Probes for Near-Infrared and Turn-on Sensing of Glutathione in Living Cells. *Langmuir* **2012**, *28*, 3945−3951.

(10) Song, X.-R.; Goswami, N.; Yang, H.-H.; Xie, J. Functionalization of Metal Nanoclusters for Biomedical Applications. *Analyst* **2016**, *141*, 3126−3140.

(11) Chwatko, G.; Kuźniak, E.; Kubalczyk, P.; Borowczyk, K.; Wyszczelska-Rokiel, M.; Głowacki, R. Determination of Cysteine and Glutathione in Cucumber Leaves by HPLC with UV Detection. *Anal. Methods* **2014**, *6*, 8039−8044.

(12) Miao, P.; Liu, L.; Nie, Y.; Li, G. An Electrochemical Sensing Strategy for Ultrasensitive Detection of Glutathione by Using Two Gold Electrodes and Two Complementary Oligonucleotides. *Biosens. Bioelectron.* **2009**, *24*, 3347−3351.

(13) McGill, M. R.; Jaeschke, H. A Direct Comparison of Methods Used to Measure Oxidized Glutathione in Biological Samples: 2-Vinylpyridine and N-Ethylmaleimide. *Toxicol. Mech. Methods* **2015**, *25*, 589−595.

(14) Zachariadis, G. A.; Rosenberg, E. Use of Modified Doehlert-Type Experimental Design in Optimization of a Hybrid Electrospray Ionization Ion Trap Time-of-Flight Mass Spectrometry Technique for Glutathione Determination. *Rapid Commun. Mass Spectrom.* **2013**, *27*, 489−499.

(15) Yin, J.; Kwon, Y.; Kim, D.; Lee, D.; Kim, G.; Hu, Y.; Ryu, J.-H.; Yoon, J. Cyanine-Based Fluorescent Probe for Highly Selective Detection of Glutathione in Cell Cultures and Live Mouse Tissues. *J. Am. Chem. Soc.* **2014**, *136*, 5351−5358.

(16) Lim, S.-Y.; Hong, K.-H.; Kim, D. I.; Kwon, H.; Kim, H.-J. Tunable Heptamethine−Azo Dye Conjugate as an NIR Fluorescent Probe for the Selective Detection of Mitochondrial Glutathione Over Cysteine and Homocysteine. *J. Am. Chem. Soc.* **2014**, *136*, 7018−7025.

(17) Kowada, T.; Maeda, H.; Kikuchi, K. BODIPY-Based Probes for the Fluorescence Imaging of Biomolecules in Living Cells. *Chem. Soc. Rev.* **2015**, *44*, 4953−4972.

(18) Yuan, X.; Tay, Y.; Dou, X.; Luo, Z.; Leong, D. T.; Xie, J. Glutathione-Protected Silver Nanoclusters as Cysteine-Selective Fluorometric and Colorimetric Probe. *Anal. Chem.* **2013**, *85*, 1913−1919.

(19) Gao, W.; Liu, Z.; Qi, L.; Lai, J.; Kitte, S. A.; Xu, G. Ultrasensitive Glutathione Detection Based on Lucigenin Cathodic Electrochemiluminescence in the Presence of MnO_2 Nanosheets. *Anal. Chem.* **2016**, *88*, 7654−7659.

(20) Niu, L.-Y.; Guan, Y.-S.; Chen, Y.-Z.; Wu, L.-Z.; Tung, C.-H.; Yang, Q.-Z. BODIPY-Based Ratiometric Fluorescent Sensor for Highly Selective Detection of Glutathione Over Cysteine and Homocysteine. *J. Am. Chem. Soc.* **2012**, *134*, 18928−18931.

(21) Yang, L.; Liu, Y.; Ma, C.; Liu, W.; Li, Y.; Li, L. Naphthalene-Fused BODIPY with Large Stokes Shift as Saturated-Red Fluorescent Dye for Living Cell Imaging. *Dyes Pigm.* **2015**, *122*, 1−47.

(22) Ge, J.; Huang, Z.-M.; Xi, Q.; Yu, R.-Q.; Jiang, J.-H.; Chu, X. A Novel Graphene Oxide Based Fluorescent Nanosensing Strategy with Hybridization Chain Reaction Signal Amplification for Highly Sensitive Biothiol Detection. *Chem. Commun.* **2014**, *50*, 11879−11882.

(23) Fleischmann, M.; Hendra, P. J.; McQuillan, A. J. Raman Spectra of Pyridine Adsorbed at a Silver Electrode. *Chem. Phys. Lett.* **1974**, *26*, 163−166.

(24) Jeanmaire, D. L.; Van Duyne, R. P. Surface Raman Spectroelectrochemistry. *J. Electroanal. Chem. Interfacial Electrochem.* **1977**, *84*, 1−20.

(25) Fang, Y.; Seong, N.-H.; Dlott, D. D. Measurement of the Distribution of Site Enhancements in Surface-Enhanced Raman Scattering. *Science* **2008**, *321*, 388−392.

DOI: 10.1021/acsanm.7b00290
ACS Appl. Nano Mater. XXXX, XXX, XXX−XXX

(26) Wang, Y.; Yan, B.; Chen, L. SERS Tags: Novel Optical Nanoprobes for Bioanalysis. *Chem. Rev.* **2013**, *113*, 1391−1428.
(27) Huang, G. G.; Han, X. X.; Hossain, M. K.; Ozaki, Y. Development of a Heat-Induced Surface-Enhanced Raman Scattering Sensing Method for Rapid Detection of Glutathione in Aqueous Solutions. *Anal. Chem.* **2009**, *81*, 5881−5888.
(28) Li, J.; Chen, L.; Lou, T.; Wang, Y. Highly Sensitive SERS Detection of as 3+Ions in Aqueous Media Using Glutathione Functionalized Silver Nanoparticles. *ACS Appl. Mater. Interfaces* **2011**, *3*, 3936−3941.
(29) Chinnakkannu Vijayakumar, S.; Venkatakrishnan, K.; Tan, B. SERS Active Nanobiosensor Functionalized by Self-Assembled 3D Nickel Nanonetworks for Glutathione Detection. *ACS Appl. Mater. Interfaces* **2017**, *9*, 5077−5091.
(30) Lee, J.; Zhang, Q.; Park, S.; Choe, A.; Fan, Z.; Ko, H. Particle−Film Plasmons on Periodic Silver Film Over Nanosphere (AgFON): a Hybrid Plasmonic Nanoarchitecture for Surface-Enhanced Raman Spectroscopy. *ACS Appl. Mater. Interfaces* **2016**, *8*, 634−642.
(31) Xu, H.; K all, M. Surface-Plasmon-Enhanced Optical Forces in Silver Nanoaggregates. *Phys. Rev. Lett.* **2002**, *89*, 246802.
(32) Macias, G.; Alba, M.; Marsal, L. F.; Mihi, A. Surface Roughness Boosts the SERS Performance of Imprinted Plasmonic Architectures. *J. Mater. Chem. C* **2016**, *4*, 3970−3975.
(33) Chen, K.-P.; Drachev, V. P.; Borneman, J. D.; Kildishev, A. V.; Shalaev, V. M. Drude Relaxation Rate in Grained Gold Nanoantennas. *Nano Lett.* **2010**, *10*, 916−922.
(34) Jane, A.; Dronov, R.; Hodges, A.; Voelcker, N. H. Porous Silicon Biosensors on the Advance. *Trends Biotechnol.* **2009**, *27*, 230−239.
(35) Xu, R.; Zhang, G.; Mai, J.; Deng, X.; Segura-Ibarra, V.; Wu, S.; Shen, J.; Liu, H.; Hu, Z.; Chen, L. An Injectable Nanoparticle Generator Enhances Delivery of Cancer Therapeutics. *Nat. Biotechnol.* **2016**, *34*, 414−418.
(36) Zhu, G.; Liu, J.-T.; Wang, Y.; Zhang, D.; Guo, Y.; Tasciotti, E.; Hu, Z.; Liu, X. In Situ Reductive Synthesis of Structural Supported Gold Nanorods in Porous Silicon Particles for Multifunctional Nanovectors. *ACS Appl. Mater. Interfaces* **2016**, *8*, 11881−11891.
(37) Harraz, F. A.; Tsuboi, T.; Sasano, J.; Sakka, T.; Ogata, Y. H. Metal Deposition Onto a Porous Silicon Layer by Immersion Plating From Aqueous and Nonaqueous Solutions. *J. Electrochem. Soc.* **2002**, *149*, C456−C458.
(38) Tsuboi, T.; Sakka, T.; Ogata, Y. H. Metal Deposition Into a Porous Silicon Layer by Immersion Plating: Influence of Halogen Ions. *J. Appl. Phys.* **1998**, *83*, 4501−4506.
(39) Huang, G. G.; Hossain, M. K.; Han, X. X.; Ozaki, Y. A Novel Reversed Reporting Agent Method for Surface-Enhanced Raman Scattering; Highly Sensitive Detection of Glutathione in Aqueous Solutions. *Analyst* **2009**, *134*, 2468−2474.
(40) Wang, C.-W.; Chang, H.-T. Sensitive Detection of Platelet-Derived Growth Factor Through Surface-Enhanced Raman Scattering. *Anal. Chem.* **2014**, *86*, 7606−7611.
(41) Yin, Y.; Li, Q.; Ma, S.; Liu, H.; Dong, B.; Yang, J.; Liu, D. Prussian Blue as a Highly Sensitive and Background-Free Resonant Raman Reporter. *Anal. Chem.* **2017**, *89*, 1551−1557.
(42) Ouyang, L.; Zhu, L.; Jiang, J.; Tang, H. A Surface-Enhanced Raman Scattering Method for Detection of Trace Glutathione on the Basis of Immobilized Silver Nanoparticles and Crystal Violet Probe. *Anal. Chim. Acta* **2014**, *816*, 41−49.
(43) Grubisha, D. S.; Lipert, R. J.; Park, H.-Y.; Driskell, J.; Porter, M. D. Femtomolar Detection of Prostate-Specific Antigen: an Immunoassay Based on Surface-Enhanced Raman Scattering and Immunogold Labels. *Anal. Chem.* **2003**, *75*, 5936−5943.
(44) Wang, F.; Widejko, R. G.; Yang, Z.; Nguyen, K. T.; Chen, H.; Fernando, L. P.; Christensen, K. A.; Anker, J. N. Surface-Enhanced Raman Scattering Detection of pH with Silica-Encapsulated 4-Mercaptobenzoic Acid-Functionalized Silver Nanoparticles. *Anal. Chem.* **2012**, *84*, 8013−8019.
(45) Wang, J.; Wu, X.; Wang, C.; Rong, Z.; Ding, H.; Li, H.; Li, S.; Shao, N.; Dong, P.; Xiao, R. Facile Synthesis of Au-Coated Magnetic Nanoparticles and Their Application in Bacteria Detection via a SERS Method. *ACS Appl. Mater. Interfaces* **2016**, *8*, 19958−19967.
(46) Tietze, F. Enzymic Method for Quantitative Determination of Nanogram Amounts of Total and Oxidized Glutathione: Applications to Mammalian Blood and Other Tissues. *Anal. Biochem.* **1969**, *27*, 502−522.
(47) Godin, B.; Chiappini, C.; Srinivasan, S.; Alexander, J. F.; Yokoi, K.; Ferrari, M.; Decuzzi, P.; Liu, X. Discoidal Porous Silicon Particles: Fabrication and Biodistribution in Breast Cancer Bearing Mice. *Adv. Funct. Mater.* **2012**, *22*, 4225−4235.
(48) Radziuk, D.; Moehwald, H. Prospects for Plasmonic Hot Spots in Single Molecule SERS Towards the Chemical Imaging of Live Cells. *Phys. Chem. Chem. Phys.* **2015**, *17*, 21072−21093.
(49) Song, J.; Yang, C.; Hu, H.; Dai, X.; Wang, C.; Zhang, H. Penetration Depth at Various Raman Excitation Wavelengths and Stress Model for Raman Spectrum in Biaxially-Strained Si. *Sci. China: Phys., Mech. Astron.* **2013**, *56*, 2065−2070.

DOI: 10.1021/acsanm.7b00290
ACS Appl. Nano Mater. XXXX, XXX, XXX−XXX